Investigation of contribution of {123} slip planes to development of rolling textures in bcc metals by use of Taylor models

D. Raabe

In order to describe the evolution of rolling textures in bcc metals, and particularly to assess the contribution of dislocation slip on {123} glide planes, a Taylor model, which makes use of increasing strain relaxation and considers various types of bcc glide system, is applied. The deformation is simulated in the range $\varepsilon = 0$–90%. The model in which dislocation slip on {110}, {112}, and {123} planes is taken into account exhibits good agreement with experimentally detected rolling textures. A comparison with computations carried out using only {110} and {112} slip planes reveals that the additionally activated {123}⟨111⟩ glide systems contributed a considerable amount of shear which was formerly attributed to the {110}⟨111⟩ and {112}⟨111⟩ slip systems.

MST/2091

 Manuscript received 25 January 1994; in final form 3 May 1994. *The author is in the Institut für Metallkunde und Metallphysik, RWTH Aachen, Germany.*

Introduction

As a result of studies over the last 50 years, the crystallographic cold rolling textures of bcc transition metals, especially Fe, Nb, Mo, V, Ta, and related alloys, were often considered to be quite similar to each other.[1–5] Only in the last 15 years, mainly by applying the three-dimensional orientation distribution function (ODF)[6], $f(g)$, instead of only two-dimensional centrosymmetric pole figures, did the studies become thorough enough to reveal characteristic differences between the cold rolling textures of various bcc metals and alloys.[7–12] In this work it was revealed that the rolling textures of bcc metals are strongly dependent on various parameters, resulting from both the specific production process and the physical mechanisms by which deformation is accomplished.

Parameters belonging to the first group are mainly technical process variables of the production steps before cold rolling. For steels these are casting conditions (continuous or strip casting),[13] hot rolling temperatures (amount of phase transformation),[14] hot rolling pass sequences, and thermomechanical treatments (evolution of through thickness inhomogeneity[15,16]). For bcc refractory metals, the combination of crossrolling and intermediate heat treatments is the main source of a non-random and inhomogeneous initial microstructure and texture.[12] All these variables lead to characteristic textures before cold rolling which are partially inherited and lead to a broad variety of subsequent cold rolling textures.

Considering the physical parameters, deformation textures are predominantly determined by the mechanisms which accomplish plastic deformation, i.e. by the type and number of active slip or twinning systems and, to a minor extent, by the microstructure, i.e. grain shape and size. Shear bands, plastic zones around precipitates, and related microstructural features, including localised plastic inhomogeneities, are considered to be of relevance mainly to microscopic texture phenomena, and will not be investigated in the present work.

Since a notable contribution by mechanical twinning has only been reported to occur in Fe–3%Si alloys,[17–19] the main factor influencing the formation of cold rolling textures in bcc transition metals must be the activated slip systems, provided that a fairly equiaxed grain structure and a weak texture are present in the initial material. Since the resulting orientation distributions are very sensitive to the activation of the various types of slip system involved, the method of texture simulation represents a very convenient tool for the quantitative investigation of the underlying mechanisms of plastic deformation during the cold rolling of bcc transition metals.

When considering the types of slip system which may be involved it is necessary to review the results stemming from corresponding single crystal experiments.[17–21] According to this work the main feature of plasticity in bcc transition metals is the occurrence of {110}, {112}, and {123} slip planes, all of which contain the $\frac{1}{2}\langle 111\rangle$ Burgers vector. Although the activation of these slip systems is widely accepted for bcc single crystal deformation, three uncertainties remain. First, it is conceded by some workers[17–21] that even by the use of transmission electron microscopy (TEM) it is not always possible to distinguish between {123} slip and combined or alternating {112} and {110} slip. Second, results stemming from TEM investigations do not generally provide statistically reliable information since – inherent to the technique – only a very small volume fraction of material is studied and the identification of a certain slip system does not yet give any information about its quantitative contribution during plastic deformation. Third, the criterion for selecting the active slip systems in polycrystals is fundamentally different from that which rules the plastic deformation of single crystals.

Accounting for these uncertainties, the application of quantitative texture analysis for the investigation of the contribution of {123} slip systems during plastic deformation of bcc metals represents a convenient addition to the quoted work.[17–21]

In a very simple test it can also be demonstrated for polycrystals that deformation is not exclusively accomplished by slip on {110} planes: the slip systems of fcc metals ($\{111\}\langle 110\rangle$) are related to the $\{110\}\langle 111\rangle$ bcc slip systems by a 90° rotation about the transverse direction. For low degrees of deformation, where local relaxation of strain constraints may be neglected, after a 90° rotation about the transverse direction the fcc textures resulting from so called ideal plane strain rolling deformation should therefore be identical to those in bcc metals. As was shown recently,[22] both types of texture are, however, only similar in their basic shape and do not show quantitative equivalence of all rotated texture components. Whereas for higher degrees of deformation in fcc metals the initial α_{fcc} fibre texture ($\{110\}\langle 001\rangle$ to $\{110\}\langle 111\rangle$) is decreased and transforms into the β fibre texture ($\{111\}\langle 112\rangle$ to $\{110\}\langle 112\rangle$), in bcc metals the initial α_{bcc} fibre is not altered but increases continuously. This fundamental

difference between the bcc and fcc textures can be attributed to the activation of additional slip systems in bcc ({112}⟨111⟩ and {123}⟨111⟩) which contribute to the stabilisation of the α_{bcc} fibre components.[22]

In recent work texture simulations have therefore been carried out, considering {110} and {112} glide planes as well as the 'pencil glide' mechanism or various simulation methods. In the thorough work by Raphanel and van Houtte[23] 'full constraints' (FC)[24] and 'relaxed constraints' (RC)[25–29] Taylor type simulations have been carried out considering {110} and {112} slip planes. For the latter type of slip system, asymmetric glide with respect to the corresponding twinning direction was considered. The authors concluded that although the introduction of RC Taylor models led to a better description of bcc rolling textures when compared with the prediction of the FC model, the relaxation which starts from the beginning of plastic deformation should be questioned. In the work of Royer *et al.*[30] a Taylor type and selfconsistent model[31] were applied, also making use of {110} and {112} slip planes. In this paper it was summarised that the RC model gives – on the basis of these glide systems – good agreement; the assumption of pencil glide, however, gives worse agreement with experimental data. In the paper by Wagner *et al.*,[32] texture simulations were carried out using RC,[25–29] FC,[24] Los Alamos Plasticity code (LAP),[33] and a viscoplastic selfconsistent model (VPSC),[34] considering {110} and {112} glide planes. It was elucidated that first, the RC and the VPSC models yielded very similar texture predictions and activated numbers of slip systems (3·2 up to 4), as well as good agreement with experimental data, and that second, the VPSC simulation did not show significant deviations if a hardening law was introduced. A shortcoming of this work is the comparison of the simulations with electrical steels, which usually reveal an increased contribution of slip on {110} glide planes owing to their higher Si content, and are therefore not representative of other bcc transition metals.

Although the main features of bcc rolling textures are described by all quoted simulations, the influence of {123} slip planes and the successive evolution of rolling texture with increasing degree of deformation (all work discussed above shows only one simulated degree of deformation) were completely neglected. Furthermore, the shear contributed by the various types of potential slip system was not quantitatively examined.

Simulation technique

In the present work the cold rolling textures of bcc transition metals will be computed by means of a Taylor model which begins the simulation of deformation under FC conditions, then concedes relaxation of the ε_{13} strain constraint (lath model), and finally also of the ε_{23} (pancake model) strain constraint. As discussed previously by Raphanel and van Houtte,[23] this successive relaxation scheme is to a certain extent arbitrary. In the present work, therefore, the impact of the relaxation scheme on the simulation results was checked quantitatively. For this purpose two schemes, i.e. an upper and lower bound estimation for the subsequent relaxation of ε_{13} and ε_{23}, respectively, have been applied. In scheme 1, FC conditions were used up to $\varepsilon = 10\%$, lath conditions in the range $\varepsilon =$ 10–30%, and the pancake model in the range $\varepsilon = 30$–90%. In scheme 2, the FC model was applied up to $\varepsilon = 30\%$, the lath model in the range $\varepsilon = 30$–60%, and the pancake model in the range $\varepsilon = 60$–90%.

In contrast to former work, {123} slip planes will also be considered in accordance with results stemming from single crystal experiments.[17–21,35–37] Although it would lead to computational simplifications, the pencil glide mechanism will not be considered here, since it leads to the application of irrational planes which is of little physical sense. For the selection of the active slip systems for non-unique solutions, the criterion by Renouard and Wintenberger was applied.[38] This criterion makes use of the introduction of small orientation deviations for the examination of the stability of the solution, which has a physical meaning since deformation grains are not oriented uniformly, but reveal considerable local orientation gradients.[39,40] In accordance with most other work, an identical critical resolved shear stress was used for all three types of slip system.

The simulation was carried out using 936 initially randomly distributed single orientations. For computing the ODFs each orientation was superimposed by a Gauss function, applying a scatter width of 8° in accordance with local orientation gradients occurring within single iron grains.[39,40] A detailed description of the main features of the Taylor theory as well as a discussion of the linear programming technique will not be given here, since these aspects have already been covered in previous work.[23–34] The simulation results will be compared with experimental findings in low C steels with almost random initial hot band textures.

Simulation results

The result of the scheme 1 simulation using {110}⟨111⟩ and {112}⟨111⟩ glide systems is shown in Fig. 1*a*. On the α fibre the uniform evolution of the orientation tube ranging from {001}⟨110⟩ to almost {111}⟨110⟩, and on the γ fibre the rise of {111}⟨110⟩ and (slightly pronounced) of {111}⟨112⟩ is revealed for $\varepsilon \leqslant 60\%$. Whereas for $\varepsilon =$ 70% the α fibre shows a similar course as for $\varepsilon < 70\%$, on the γ fibre a transition from {111}⟨112⟩ to {111}⟨110⟩ is detected. For $\varepsilon = 80\%$ on the α fibre a weak maximum close to {111}⟨110⟩ at $\phi = 48°$ is developed. On the γ fibre the maximum is stabilised at {111}⟨110⟩ whereas {111}⟨112⟩ is decreased. The simulation for $\varepsilon = 90\%$ leads on the α fibre to a narrow maximum close to ~{111}⟨110⟩ at $\phi \approx 48°$. A second peak is developed at {001}⟨110⟩ and a third weak component is indicated at ~{113}⟨110⟩ ($\phi \approx 22°$).

The scheme 1 simulation in which {123}⟨111⟩ glide systems are also considered is shown in Fig. 1*b*. For $\varepsilon \leqslant 50\%$ the texture is very similar to that predicted by the simulation using {110}⟨111⟩ and {112}⟨111⟩ glide systems (Fig. 1*a*). On the α fibre, however, a slight preference of the {112}⟨110⟩ texture component is indicated (Fig. 1*b*). During deformation the evolution of a broad maximum at {112}⟨110⟩, which is slightly shifted towards $\phi \approx 40°$ at $\varepsilon = 90\%$, can be seen. Additionally, a second maximum occurs at {001}⟨110⟩. On the γ fibre, a similar development as for the {110} and {112} slip planes is revealed, i.e. the maximum is shifted from {111}⟨112⟩ towards {111}⟨110⟩, although it does not become as sharp as in Fig. 1*a*.

When the above simulations are carried out using scheme 2 and considering {110} and {112} slip planes (*see* Fig. 1*c*), the texture is similar to that predicted by scheme 1. On the α fibre, however, the previously observed maxima at {001}⟨110⟩ and ~{113}⟨110⟩ (Fig. 1*a*) are considerably decreased, and on the γ fibre the initially occurring {111}⟨112⟩ ($\varepsilon \leqslant 70\%$) as well as the subsequent maximum {111}⟨110⟩ ($\varepsilon > 70\%$) are more pronounced.

The scheme 2 simulation (*see* Fig. 1*d*) also shows slight deviations from the scheme 1 predictions (Fig. 1*b*) for the {110}, {112}, and {123} slip planes. Although the maximum on the α fibre is still located close to {112}⟨110⟩ ($\phi \approx 40°$),

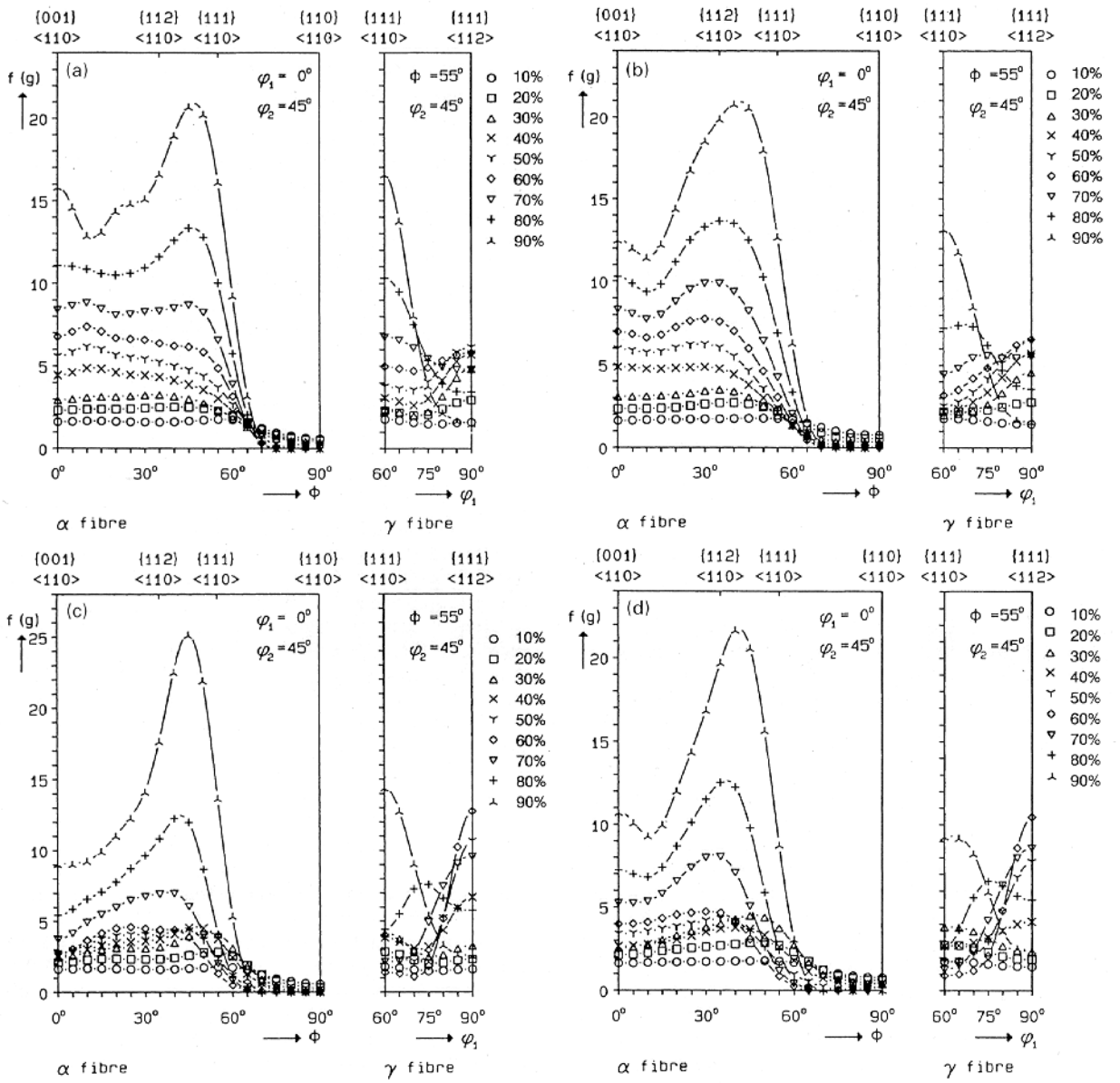

a, c {110}⟨111⟩ and {112}⟨111⟩; *b, d* {110}⟨111⟩, {112}⟨111⟩, and {123}⟨111⟩

1 Simulated evolution of bcc rolling textures using various different slip systems (successive strain relaxation) using *a, b* scheme 1 ($\varepsilon = 0$–10% full constraints (FC), $\varepsilon = 10$–30% lath, $\varepsilon = 30$–90% pancake), and *c, d* scheme 2 ($\varepsilon = 10$–30% FC, $\varepsilon = 30$–60% lath, $\varepsilon = 60$–90% pancake)

it is less broad and the {001}⟨110⟩ component is weaker ($\varepsilon = 90\%$). On the γ fibre the maximum {111}⟨112⟩ ($\varepsilon \leqslant 70\%$) as well as the following peak {111}⟨110⟩ ($\varepsilon > 70\%$) are sharper.

Experimental technique and results

As an example of a typical bcc transition metal with a nearly random starting texture ($f(g)_{max} = 4$ at {001}⟨110⟩), a small grain size (~ 12 μm), and negligible plastic inhomogeneities, the evolution of the rolling texture of a low C deep drawing steel was examined. As has been discussed previously,[8–16] the observed weak {001}⟨110⟩ orientation in the starting material is assumed to result from the hot rolling process, since during the last one or two rolling passes incomplete recrystallisation, and during subsequent cooling insufficient phase transformation, occurs. Other relevant initial orientations do not occur. This phenomenon, which is attributed to the decrease in hot rolling temperature for low C steels, also causes a more elongated rather than a completely equiaxed grain morphology.

After industrial hot rolling, the material was cold rolled on a laboratory rolling mill in a strictly reversing manner, i.e. the sample was rotated 180° about the transverse direction after each pass. Since homogeneous deformation is determined primarily by the ratio of the contact length between the strip and the roll surface l_d to the sheet thickness d, a ratio of $1 < l_d/d < 3$ was obtained during cold rolling. The texture and microstructure of bcc materials is often inhomogeneous through the sheet thickness.[15,16,41] The initial hot and cold rolled samples were thus examined in various through thickness layers. In the present instance, however, no texture gradients between various layers were detected. All experimental textures were therefore taken from the midthickness layer.

All textures have been quantitatively examined by measuring the four incomplete pole figures {110}, {200}, {112}, and {103} within the range of the pole distance angle α (5–85°) with Mo $K_{\alpha 1}$ radiation in the back reflection mode,[42] and by deriving from them the ODF $f(g)$

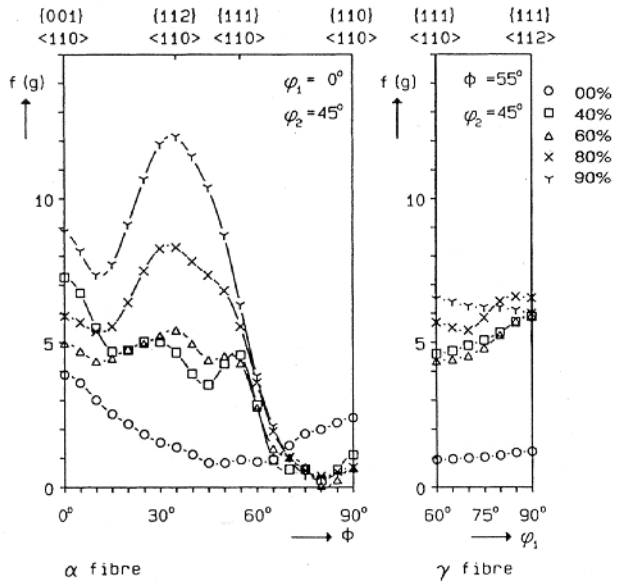

2 Experimentally achieved rolling textures of low C steel

($l_{max} = 22$) using the series expansion method (the orientation g is given here in terms of the Euler angles φ_1, Φ, and φ_2).[6] For correction of 'ghost' errors which result from the absence of the odd coefficients of the series expansion, the calculated ODFs were approximated by model ODFs.[43] According to the cubic crystal symmetry and the orthorhombic sample symmetry (RD = rolling direction, ND = normal direction, TD = transverse direction), the textures are presented in the reduced Euler space ($0° \leqslant \varphi_1$, ϕ, $\varphi_2 \leqslant 90°$). Since bcc metals tend to develop texture fibres, it is convenient to present the orientation density along various fibres. The most relevant orientations are accumulated along the α fibre, $\{hkl\}\langle 110\rangle$, and along the γ fibre, $\{111\}\langle uvw\rangle$.

The cold rolling textures of the steel investigated reveal two main features, namely the formation of a strong incomplete α fibre and the increase of the γ fibre (*see* Fig. 2). For $\varepsilon < 80\%$ the formation of a continuous orientation tube ranging from $\{001\}\langle 110\rangle$ to $\{111\}\langle 110\rangle$ (α fibre) is observed. After $\varepsilon = 80\%$ the texture maximum ranges from $\{112\}\langle 110\rangle$ to almost $\{111\}\langle 110\rangle$. With continuing deformation ($\varepsilon = 90\%$) the $\{112\}\langle 110\rangle$ component becomes the absolute texture maximum which is accompanied by a weaker peak at $\{001\}\langle 110\rangle$. Despite the occurrence of these two maxima the texture can, however, by characterised as fibre type and not as peak type. On the uniformly developed γ fibre for $\varepsilon < 80\%$ a weak preference for $\{111\}\langle 112\rangle$ is revealed. For $\varepsilon \geqslant 80\%$ the maximum is shifted to $\{111\}\langle 110\rangle$ (Fig. 2). The depicted texture evolution is typical for cold rolling of bcc transition metals,[8–12] provided that a nearly random orientation distribution was present before cold rolling.

Discussion

Comparison of the predicted (Fig. 1) and experimentally achieved (Fig. 2) texture development reveals that the simulation with {110}, {112}, and {123} glide planes which was carried out according to scheme 1 (Fig. 1*b*) exhibits the best agreement with the measured data. The occurrence of two distinct maxima on the α fibre, their ϕ coordinates, the scatter width of the texture components, and the subsequent evolution of the $\{111\}\langle 112\rangle$ and $\{111\}\langle 110\rangle$ orientations on the γ fibre reveal very good agreement with the experimentally observed textures (Fig. 2).

The occurrence of a weak $\{001\}\langle 110\rangle$ component in the initial texture does obviously not have a major influence on further texture evolution. The increase in the $\{001\}\langle 110\rangle$ orientation during cold rolling is in good agreement with the simulation (Fig. 1*b*). The main inaccuracy in the simulation is the sharpness of the texture, which predicts higher ODF values when compared to those observed. This quantitative deviation of the predicted texture is dependent on the applied scatter width of the superimposed Gauss functions. A further enhancement of the applied scatter width (8°) would, however, only lead to an artificial flattening of the simulated texture without a sound physical basis.[39,40]

All Taylor type theories contain the fundamental shortcoming that the activated dislocations are reduced to their purely geometrical function, i.e. dislocation dynamics are not considered. Whereas the effect of the changing aspect ratio of the grains can be treated artificially as in the present instance, the absence of dislocation dynamics implies that related effects such as hardening, influence of cell size, and the occurrence of mesoscopic inhomogeneities such as micro- and shear bands which all affect the texture development in terms of quantitative (rotation velocity, texture maximum) and qualitative deviations (stable orientations) are neglected. From this viewpoint, the good agreement between simulation and experiment is even surprising. It has, however, been reported by Wagner *et al.*[32] that the implementation of a hardening law into a viscoplastic selfconsistent model also did not lead to essential changes in the predicted textures. These observations thus allow the conclusion that (for bcc metals) the basic texture evolution of homogeneous materials is only weakly related to the microstructure within each single grain, and the main influence has to be attributed to the types of potential slip system and the subsequent relaxation of strain constraints. Concerning the 'kinetics' of texture evolution, however, the microstructure is nevertheless expected to be of relevance.

A strong impact of the grain morphology was demonstrated for texture evolution in ferritic stainless steels[11,12,15] and transformer steels.[16] In the hot band material, a through thickness gradient of the texture and the grain morphology is evident. In the centre layers both types of steel reveal the occurrence of a strong α fibre after hot rolling and an elongated and recovered grain structure, i.e. the absence of massive recrystallisation. During subsequent cold rolling, the formation of a strong maximum close to $\{111\}\langle 110\rangle$ on the γ fibre is observed in both alloys without the preceding formation of a maximum at $\{111\}\langle 112\rangle$. This texture evolution is attributed to the physical relaxation of the ε_{13} and ε_{23} strain constraints already present from the beginning of cold rolling owing to the flattened grain structure stemming from hot rolling.

The scheme 2 simulation with {110}, {112}, and {123} glide planes (Fig. 1*d*) also shows good agreement with experiment, although the predicted texture components show a lower scatter width than those observed experimentally. This result indicates that the assumption that strain relaxation has already begun at low degrees of deformation (scheme 1) seems more reasonable. It has to be stressed, however, that the start of strain relaxation at such low degrees of deformation is not exclusively dependent on the grain morphology. This becomes evident when the deformation of polycrystals is discussed using two opposite cases. In the first case the externally imposed strains are entirely accomplished by crystallographic slip, making use of five active slip systems. Consequently, grain interaction does not take place. The number of active slip systems, however, leads to a high value of deformation energy. In the opposite case a lower number of slip systems are active, implying that local strain relaxation has to be conceded which may lead to an increase in the grain interaction energy. The

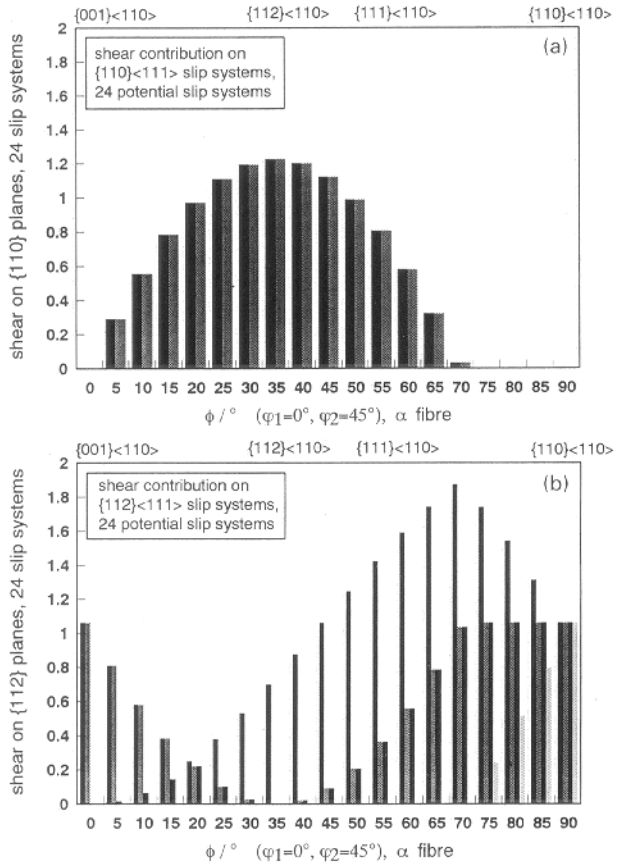

3 Shear contribution during rolling deformation of *a* {110}⟨111⟩ and *b* {112}⟨111⟩ slip systems (α fibre orientations)

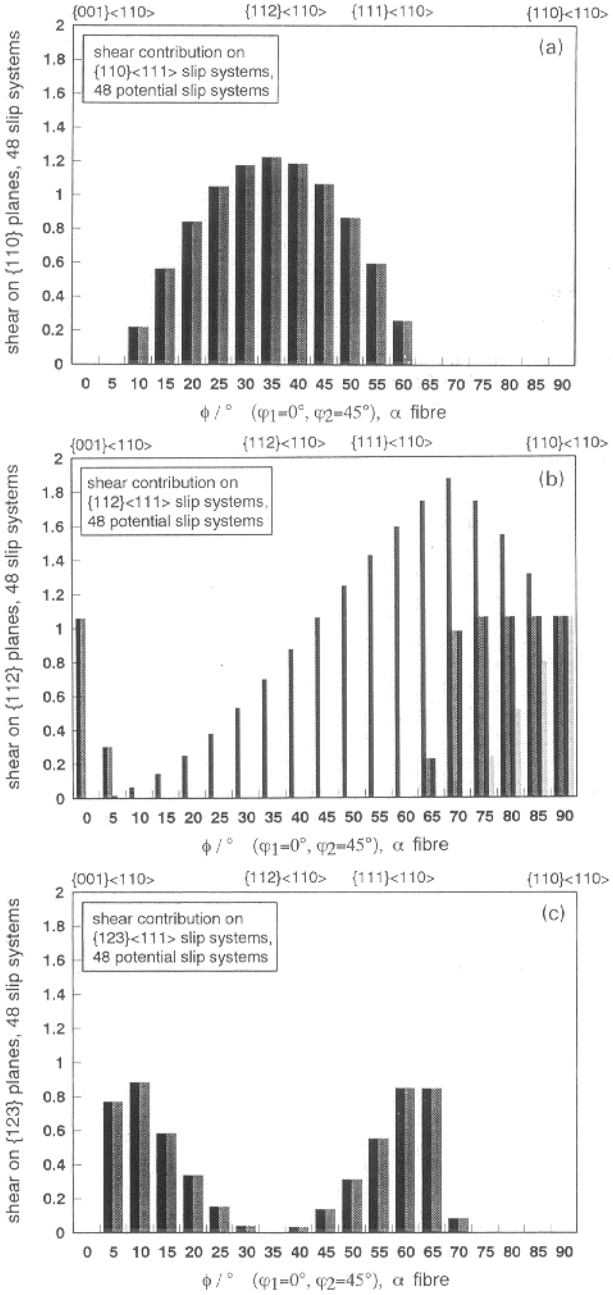

4 Shear contribution during rolling deformation of *a* {110}⟨111⟩, *b* {112}⟨111⟩, and *c* {123}⟨111⟩ slip systems (α fibre orientations)

internal deformation energy, however, is decreased. This comparison shows that the allowance for strain relaxation is not simply ruled by the grain morphology but also by the relationship between the internal deformation energy and the energy resulting from grain interaction.

Although the best agreement between experimental observation and texture prediction was achieved for {110}, {112}, and {123} glide planes (Fig. 1*b*), the texture which is computed using only {110} and {112} planes (Fig. 1*a*) also shows some features which correspond to the measured data (Fig. 2). The main inaccuracies in this prediction are, however, the occurrence of a maximum at ~{113}⟨110⟩, the narrow maximum close to {112}⟨110⟩ as well as its deviation from the observed position ($\phi \approx 35°$), and the exaggerated increase of {111}⟨110⟩ on the γ fibre. Even stronger deviations occur if the simulations are carried out according to scheme 2 (Fig. 1*c*).

In order to investigate which types of slip system contribute to the simulated deformation, the executed shear is plotted for all active slip systems (Figs. 3 and 4). For this estimation only one deformation step of $\varepsilon = 1\%$ was carried out under FC conditions. It is revealed that for {110} and {112} slip planes (Fig. 3), the contribution of two activated {110}⟨111⟩ glide systems is dominant in the range of the broad maximum close to the {112}⟨110⟩ texture component (Fig. 3*a*). The {112}⟨111⟩ slip systems mainly contribute to the deformation of the texture components at {001}⟨110⟩ and {111}⟨110⟩ and for components with higher ϕ values (Fig. 3*b*).

Concerning the activation of {110}⟨111⟩ and {112}⟨111⟩ slip systems, similar results are achieved if {110}, {112}, and {123} slip planes are taken into account (Fig. 4). Two slip systems with {110} planes contribute to the deformation of texture components in the broad range close to {112}⟨110⟩ (Fig. 4*a*). The {112}⟨111⟩ slip systems contribute to the deformation of the texture components at {001}⟨110⟩ and {111}⟨110⟩ and of components with higher ϕ values (Fig. 4*b*). It is, however, revealed that the {123}⟨111⟩ slip systems also contribute a considerable amount to the total shear (Fig. 4*c*). When compared with the simulations depicted in Fig. 3, the shear on {123}⟨111⟩ systems stems from former contributions of both {110}⟨111⟩ and {112}⟨111⟩ slip systems. This result therefore indicates that if {123}⟨111⟩ glide systems are also taken into consideration, competition occurs not only between slip on {123} and {112} planes but also between {123} and {110} planes.

Conclusions

In the present work a modified Taylor model has been applied to simulate the rolling deformation of bcc metals

in the range $\varepsilon = 0$–90%. In this approach the imposed strain was successively relaxed in accordance with the increasing aspect ratio of the grains. The model which used (i) the activation of dislocation slip on {110}, {112}, and {123} planes and (ii) the FC model from $\varepsilon = 0$–10%, the lath model from $\varepsilon = 10$–30%, and the pancake model from $\varepsilon = 30$–90%, revealed the best correspondence to the experimentally observed textures.

References

1. G. WASSERMANN and J. GREWEN: 'Texturen metallischer Werkstoffe'; 1962, Berlin, Springer-Verlag.
2. I. L. DILLAMORE and W. T. ROBERTS: *Acta Metall.*, 1964, **12**, 281.
3. F. HAESSNER and D. MAYER-ROSA: *Z. Metallkd.*, 1967, **58**, (H1), 12.
4. I. L. DILLAMORE, C. J. E. SMITH, and T. W. WATSON: *Met. Sci.*, 1967, **1**, 49.
5. I. L. DILLAMORE and H. KATOH: *Met. Sci.*, 1974, **8**, 21.
6. H. J. BUNGE: *Z. Metallkd.*, 1965, **56**, 872.
7. H. J. BUNGE: *Kristall Tech.*, 1970, **5**, 145.
8. C. DÄRMANN, S. MISHRA, and K. LÜCKE: *Acta Metall.*, 1984, **32**, 2185.
9. U. von SCHLIPPENBACH, F. EMREN, and K. LÜCKE: *Acta Metall.*, 1986, **34**, 1289.
10. M. MATSUO: *ISIJ Int.*, 1989, **29**, (10), 809.
11. M. HÖLSCHER, D. RAABE, and K. LÜCKE: *Steel Res.*, 1991, **62**, (12), 567.
12. D. RAABE, K. LÜCKE, and G. GOTTSTEIN: *J. Phys. (France) IV, (Colloque C7)*, November 1993, **3**, 523.
13. D. RAABE, M. HÖLSCHER, M. DUBKE, H. PFEIFER, H. HANKE, and K. LÜCKE: *Steel Res.*, 1993, **64**, (7), 359.
14. R. K. RAY and J. J. JONAS: *Int. Mater. Rev.*, 1990, **35**, 1.
15. D. RAABE and K. LÜCKE: *Mater. Sci. Technol.*, 1993, **9**, (4), 302.
16. L. SEIDEL, M. HÖLSCHER, and K. LÜCKE: *Textures Microstruct.*, 1989, **11**, 171.
17. B. SESTÁK and A. SEEGER: *Z. Metallkd.*, 1978, **69**, (4), 195.
18. B. SESTÁK and A. SEEGER: *Z. Metallkd.*, 1978, **69**, (6), 355.
19. B. SESTÁK and A. SEEGER: *Z. Metallkd.*, 1978, **69**, (7), 425.
20. J. W. CHRISTIAN: *Metall. Trans.*, 1983, **14A**, 1237.
21. C. N. REID: *Acta Metall.*, 1966, **14**, 13.
22. M. HÖLSCHER, D. RAABE, and K. LÜCKE: *Acta Metall.*, 1994, **42**, 879.
23. J. L. RAPHANEL AND P. van HOUTTE: *Acta Metall.*, 1985, **33**, 1481.
24. G. I. TAYLOR: *J. Inst. Met.*, 1938, **62**, 307.
25. H. HONNEFF and H. MECKING: in Proc. 5th. Conf. on 'Texture of materials' (ICOTOM 5), (ed. G. Gottstein and K. Lücke), 265; 1978, Berlin, Springer-Verlag.
26. H. HONNEFF and H. MECKING: in Proc. 6th Int. Conf. on 'Texture of materials' (ICOTOM 6), (ed. S. Nagashima), 347; 1981, Tokyo, Iron and Steel Institute of Japan.
27. U. F. KOCKS and H. CHANDRA: *Acta Metall.*, 1982, **30**, 695.
28. R. G. CANOVA, U. F. KOCKS, and J. J. JONAS: *Acta Metall.*, 1984, **32**, 211.
29. P. van HOUTTE: in Proc. 6th Int. Conf. on 'Texture of materials' (ICOTOM 6), (ed. S. Nagashima), 428; 1981, Tokyo, Iron and Steel Institute of Japan.
30. F. ROYER, A. NADARI, F. YALA, P. LIPINSKI, D. CECCALDI, M. BERVEILLER, and P. PENELLE: *Textures Microstruct.*, 1991, **14–18**, 1129.
31. P. LIPINSKI and M. BERVEILLER: *Int. J. Plast.*, 1989, **5**, 149.
32. F. WAGNER, G. CANOVA, P. van HOUTTE, and A. MOLINARI: *Textures Microstruct.*, 1991, **14–18**, 1135.
33. U. F. KOCKS: in Proc. 8th Int. Conf. on 'Texture of materials' (ICOTOM 8), (ed. J. Kallend and G. Gottstein), 285; 1987, Warrendale, PA, The Metallurgical Society of AIME.
34. A. MOLINARI, R. G. CANOVA, and S. AHZI: *Acta Metall.*, 1987, **35**, 2983.
35. D. VESELY: *Phys. Status Solidi*, 1969, **29**, 675.
36. P. G. SMERD: DPhil thesis, University of Oxford, 1968.
37. K. JORDAN and N. STOLOFF: *Trans. Jpn Inst. Met. (Suppl.)*, 1968, **9**, 281.
38. M. RENOUARD and M. WINTENBERGER, *C.r. Acad. Sci.*, 1976, **B283**, 237.
39. D. RAABE: *Phys. Status Solidi (b)*, 1994, **181**, 291.
40. J. BOESLAU and D. RAABE: *Mater. Sci. Forum*, 1994, 157–162, 501–506.
41. D. RAABE and K. LÜCKE: *Scr. Metall.*, 1992, **26**, 1221.
42. L. G. SCHULZ: *J. Appl. Phys.*, 1949, **20**, 1030.
43. K. LÜCKE, J. POSPIECH, K. H. VIRNICH, and J. JURA: *Acta Metall.*, 1981, **29**, 167.